PHYSICAL REVIEW B VOLUME 24, NUMBER 6 15 SEPTEMBER 1981

First-principles electronic structure of Si, Ge, GaP, GaAs, ZnS, and ZnSe. I. Self-consistent energy bands, charge densities, and effective masses

C. S. Wang
Department of Physics and Astronomy, University of Maryland, College Park, Maryland 20742 and Naval Research Laboratory, Washington, D. C. 20375

B. M. Klein
Naval Research Laboratory, Washington, D. C. 20375

(Received 18 March 1981; revised manuscript received 13 May 1981)

The self-consistent electronic structures of Si, Ge, and zinc-blende GaP, GaAs, ZnS, and ZnSe have been determined using the linear combination of Gaussian orbitals method with a local-density form of the exchange-correlation functional. A completely general form of the spatial dependence of the potential has been used to describe accurately the bonding character in the tetrahedral environment. Results are presented for the valence- and conduction-band energies, densities of states, effective masses, and charge densities. Comparisons are made with previous calculations and with photoemission measurements. A striking result is that the local-density theory underestimates the optical band gaps by approximately 30% or more, although the general conduction-band topology is good. The theoretical valence-band energies, charge densities, and electron and hole effective masses are also in good agreement with experiment. The energies and wave functions presented here are used to determine the optical properties of these materials in the following paper.

I. INTRODUCTION

The present study was motivated by the need to ascertain the efficacy of present-day self-consistent energy-band theory in describing the electronic structures (including excitation spectra) of representative semiconductors. The materials we have chosen to study are Si and Ge in the diamond structure, and GaP, GaAs, ZnS, and ZnSe in the zinc-blende structure. These materials were chosen for several reasons: (1) due to their technological importance they are well studied experimentally, (2) there is a long history and theoretical literature regarding most of them, and (3) the maximum atomic number is 34 (for Se) so that relativistic effects, neglected in our calculations, are relatively unimportant. A comprehensive study such as this is particularly appropriate at the present time as the local-density (LD) theory of electron systems is now well developed and relatively unambiguous. Previous studies of semiconductors have usually been limited either because of their empirical nature,[1-5] non-self-consistency,[6-10] or the propensity for arbitrarily varying the form of the exchange-correlation potential to fit some aspect of the experimental results (often the valence-conduction—band gaps) at the expense of theoretical rigor and the concomitant errors in other parts of the electronic spectrum and charge density.[11-17] Furthermore, many of the previous calculations have made approximations to the shape of the total potential (muffin tins, overlapping spheres, etc.,[6-8,18-22]) which leads to possible errors in the electronic structure which are largely not understood. The present calculations using the self-consistent (SC) linear combination of Gaussian orbitals (LCGO) method, and other recent *ab initio* calculations,[23,24] avoid these pitfalls and may be considered state-of-the-art applications of the LD theory for semiconductor systems. This is extremely important, as attempts to go beyond one-electron LD theory in describing, for instance, excitation spectra should be based on sound LD ground-state calculations in order to avoid being misleading.

We have chosen to divide our work into two papers for clarity. The present paper is mainly concerned with describing the results of our ground-state energy-band calculations for the six semiconductors, while the second following paper (to be re-

ferred to as II) gives a thorough discussion of our calculated optical properties and compares and discusses the agreement with experiment. There are six sections in the present paper: Section II describes the LCGO methodology used in performing the band-structure calculations; Sec. III gives results of the energy bands and densities of states including a comparison with other theoretical results; Sec. IV discusses our results for photoemission spectra and compares with experiment; Sec. V deals with our calculated hole and electron effective masses and their experimental counterparts; while in Sec. VI we present our results for the ground-state charge densities and the resultant bonding, and again we compare with the available experimental data.

II. METHODOLOGY

The linear combination of Gaussian orbital (LCGO) method[25,26] has been successfully applied, self-consistently, within the local-density-functional formalism to study the electronic properties of a wide range of simple[27,28] and transition metals[29–31] and a few covalently bonded materials.[32] The essential features of the computational technique together with a detailed account of the computer programs for cubic monoatomic crystals have been published elsewhere.[33] Here we will give a brief discussion of the procedure that we have adopted for a more general system with more than one atom per unit cell and nonsymmorphic group symmetry.

A. Linear combination of Gaussian orbital basis

The optimum choice of a LCGO basis set which provides maximum variational freedom yet still maintains a manageable size of the secular equation has been the subject of numerous discussions.[34] In our study for covalently bonded diamond and zinc-blende materials we have chosen a linear combination of atomic orbitals *minimum* basis set with an additional shell of s, p, and d virtual Gaussian-type orbitals (GTO) for added variational flexibility. The atomic orbitals were solutions to the atomic secular equation constructed with the self-consistent Herman-Skillman atomic potential[35] and a basis set of GTO. The Gaussian exponents were varied nonlinearly to minimize the atomic energies as follows: We first construct Gaussian wave functions which minimize the atomic $1s$, $2p$, or $3d$ state energies following the procedure of Euwema.[36] For each angular momentum we add two more extended GTO to minimize the energies of the next lowest states. This procedure is continued until all valence states of the atom are completed. The atomic orbitals were then augmented by an additional s, p, and d shell of independent GTO for the variational freedom needed to describe the wave functions in a solid. The presence of these diffuse GTO often leads to approximate linear dependence of the basis set, hence the overlap matrices must be checked carefully against negative or unphysically small eigenvalues throughout the Brillouin zone. We find it helpful to truncate the tail of the highest valence atomic orbitals by setting minimum values for the corresponding Gaussian exponents. Variationally, this has little effect because the long tail of the atomic orbitals are strongly modified in a solid by the overlap of the wave functions on the neighboring atomic sites. These changes can only be fitted with the aid of the additional virtual orbitals. The resulting basis set is not complete but does overlap both the bounded and low excited subspace of the wave functions. It leads to a dimension of 36×36 for the secular equation for Si, 45×45 for GaP and ZnS, and 54×54 for Ge, GaAs, and ZnSe.

B. Crystal potential

The initial Coulomb potential is constructed as a superposition of overlapping spherically symmetric atomic potentials. The corresponding overlapping atomic charge density is used to evaluate the local-density exchange-correlation potential which we choose to be a Wigner interpolation formula[37] of the form (energies are in Ry)

$$V_{\mathrm{xc}}(\vec{r}) = -2\left[\frac{3}{\pi}\right]^{1/3}\rho^{1/3}\left[1.0+\frac{(0.0569\rho^{1/3}+0.0060}{(\rho^{1/3}+0.079)^2}\right], \tag{1}$$

where the charge density ρ is evaluated at the point $\vec{r}$. This form of the Wigner interpolation formula is numerically nearly identical to the one used by Hamann[23] in his Si band-structure calculations to be discussed in Sec. III C. Owing to the analytic properties of the Gaussian orbitals it is customary to expand the crystal potential in a set of either symmetrized plane waves (SPW) or overlapping GTO.

The plane-wave basis has the advantage of being completely general, but has the disadvantage of slowly converging near the nuclei due to the Coulomb singularity. For example, even with the aid of an Ewald-type procedure, it is necessary to include 4000 stars of reciprocal lattice vectors to describe the crystal potential for Ni (Ref. 29) and Fe.[30] For a more complex structure with less symmetry such a procedure can be prohibitively expensive. The GTO, on the other hand, converge rather rapidly (fewer than 20 GTO are needed to describe an atomic potential to good accuracy). However, overlapping spherical GTO are too spherical around each atom to describe the directional bond in a covalent material. Although results can be improved by including higher angular momentum terms around each atom and/or additional GTO centered at the interstitial tetrahedral sites, such a procedure is somewhat arbitrary compared to the Fourier series expansion, where the reciprocal lattice vectors are rigorously defined. Thus we choose to expand our potential in a mixed basis of GTO and SPW as proposed by Euwema.[36] The self-consistent Herman-Skillman neutral atomic Coulomb and exchange-correlation potential are each fitted with 18 even-tempered GTO.[36] The four longest range GTO which can be represented by rapidly converging Fourier series are deleted to avoid excessive lattice sums in constructing the overlapping crystal potential. The difference between the exact atomic Coulomb potential and the truncated GTO series are tabulated over a logarithmatic radial mesh and their Fourier coefficients calculated numerically. In general, the crystal $V_{xc}(\vec{r})$ cannot be expressed as a superposition of atomic $V_{xc}(\vec{r})$. However, subtracting out the contribution from the overlapping atomic GTO series helps to eliminate the cusp behavior near the nuclei to yield a rapidly converging Fourier expansion. Typically, 25 independent Fourier coefficients were evaluated via a three-dimensional least-squares fitting procedure based on a sampling of 400 random points in the unit cell. Once the expansion coefficients of the potential are known, the Hamiltonian matrices can be evaluated analytically, the secular equation is solved, and we are ready to find the self-consistent potential.

C. Self consistency

The major modification in the charge density due to self-consistency (charge transfer, change in valence electron s and p concentration, etc.) are expected to occur in the interstitial region, particularly along the tetrahedral bond. Therefore the Gaussian expansion describing the atomic potential near the nucleus is kept frozen at their starting values; only the Fourier coefficients are varied following the procedure of Callaway and Fry.[38] At the lth iteration, the Fourier coefficients of the input Coulomb potential $V_C(\vec{K}_s)$ are evaluated from the output charge density $\rho(\vec{K})$ of the $(l-1)$th iteration, with

$$V_C(\vec{K}_s) = \frac{8\pi}{K_s^2}\rho(\vec{K}_s) , \tag{2}$$

and $\rho(\vec{K}_s)$ calculated analytically from the wave functions

$$\rho(\vec{K}_s) = \sum_{n\vec{k}} C_{ni}^*(\vec{k}) C_{nj}(\vec{k}) S_{ij}(\vec{k},-\vec{K}_s) . \tag{3}$$

Here the sum runs over all occupied bands (index n) and wave vectors $\vec{k}$, $c_{ni}(\vec{k})$ are the eigenvectors, and the generalized overlap matrices

$$S_{ij}(\vec{k},\vec{K}_s) = \int \phi_i^*(\vec{k},\vec{r}) e^{i\vec{K}_s\cdot\vec{r}} \phi_j(\vec{k},\vec{r}) d^3r \tag{4}$$

are simply the matrix elements of the plane waves calculated between the basis functions $\phi_i(\vec{k},\vec{r})$. Ten special $\vec{k}$ points[39] in the $\frac{1}{48}$th of the irreducible Brillouin zone were used in our iterations for a self-consistent potential. In order to speed up the convergence, $\rho(\vec{K}_s)$ is relaxed by mixing with 50% of the input $\rho(\vec{K}_s)$ at the $(l-1)$'s iteration before they are substituted into Eq. (2). Once $\rho(\vec{K}_s)$ has been determined it is straightforward to calculate $\rho(\vec{r})$ and hence the exchange-correlation potential at the selected points in the unit cell. The contribution from the overlapping GTO are subtracted before the new Fourier coefficients $V_{xc}(\vec{K}_s)$ are determined by a three-dimensional least-squares fitting procedure. Finally, the plane-wave contributions of both the Coulomb and the exchange-correlation potential to the new Hamiltonian are calculated via

$$H_{ij}(\vec{k}) = \sum_{\vec{K}_s} [\, V_C(\vec{K}_s) + V_{xc}(\vec{K}_s)] \times S_{ij}(\vec{k},\vec{K}_s) , \tag{5}$$

where $S_{ij}(\vec{k},\vec{K}_s)$ is the same matrix used in Eq. (3) to evaluate $\rho(\vec{K}_s)$ which has been calculated once and for all before the self-consistent cycles begin. We found $\rho(\vec{K}_s)$ converges to within 10^{-4} a.u. and the energies to 0.02 eV at the end of 5 iterations. Once the self-consistent potential is determined, the energies and wave functions are tabulated at 89 equally spaced points in $\frac{1}{48}$th of the Brillouin zone in order to calculate the density of states and the optical properties (including the matrix elements) presented in the following sections and paper II,

respectively. The tetrahedral integration method[40] was used in these calculations.

III. BAND STRUCTURES AND DENSITIES OF STATES

In Table I we list the lattice constants used in our calculations, while Figs. 1—6 show the energy bands and densities of states $[N(E)]$ of Si, Ge, GaP, GaAs, ZnS, and ZnSe, respectively. Table II gives a tabulation of energy eigenvalues at the symmetry points Γ, X, and L for all six materials; a more complete list of results on the 89-point mesh is available from the authors.[41] As can be seen from Figs. 1 and 2 and Figs. 3—6 the energy bands and $N(E)$ of the diamond structure elements Si and Ge are very similar, as are the results for the zinc-blende compounds; we discuss the two sets of results separately.

A. Si and Ge results

From Figs. 1 and 2 we see that the sp^3 valence bands of the homopolar semiconductors Si and Ge are gapless with the lower energy states (e.g., near Γ_1^v) being mainly s-like and the upper valence bands being dominated by p-like character (by inspection of the LCGO eigenfunctions). Both Si and Ge are calculated to be indirect-gap semiconductors with their indirect gaps being $\Gamma_{25'}^v - \Delta_1^c$ and $\Gamma_{25'}^v - L_1^c$, respectively. The indirect and lowest direct gaps are listed in Table III. All of the gaps are significantly smaller than the values observed in optical measurements, although the calculated symmetry assignments of the conduction-band states appear to be correct in all cases. In particular, the ordering of the Γ_{15}^v and $\Gamma_{2'}^c$ states, opposite for Si and Ge, is correctly predicted in both cases. We note that the $\Gamma_{2'}$ state of predominant s character is very localized around the Si or Ge site, and its eigenvalue is sensitive to variations in the SC potential due to exchange-correlation, relativistic effects, or other approximations in the theory. Further comparisons and discussion of the calculated conduction-band states with optical measurements are presented in paper II.

B. GaP, GaAs, ZnS, and ZnSe results

The energy bands and $N(E)$ of the heteropolar zinc-blende structure compounds are shown in Figs. 3—6. As can be seen the overall topology of the energy bands of all four compounds are very similar, but they have some important differences. First we note that in the zinc compounds the $3d$ bands of Zn fall in the middle of the sp valence-band manifold, in particular, in the heteropolar valence-band gap. The Ga $3d$ bands (not shown) are several electron volts below the lowest sp valence-band energy (see Sec. IV). The several electron volt heteropolar valence-band gap between the lower and upper sp valence bands is related to the absence of an inversion center in the zinc-blende lattice and the electronegativity difference between the cations (Zn or Ga) and anions (P, As, S, or Se). The occupied valence states are somewhat dominated by anion electrons, with the lowest band being primarily s-like and the upper band being p-like. Further discussion of the bonding and charge density will be given in Sec. VI. All but GaP are calculated to be direct- $(\Gamma_{15}^v - \Gamma_1^c)$ gap semiconductors. In the case of GaP, the lowest gap is $\Gamma_{15}^v - \Delta_1^c$, similar to Si. All of the gaps are given in Table III, where, as in the case of Si and Ge, the calculated gaps are systematically smaller than those determined from optical measurements, although the conduction-band topology is in accord with experiment. An example of a subtle aspect of the calculated conduction bands of GaAs and GaP are the relative positions of the lowest L_1^c and X_1^c states in these two compounds. As can be seen from Table II and Figs. 3 and 4 the ordering in GaP is X_1^c, L_1^c, and opposite in GaAs, a result in agreement with experiment.[42—44] In particular, we find that L_1^c lies 241 meV below X_1^c, in GaAs, in fairly good agreement with the experimental results of Aspnes *et al.*[42] who find the value 170 ± 30 meV.

TABLE I. Cubic lattice constants, a, used in the energy-band calculations.

	Si	Ge	GaP	GaAs	ZnS	ZnSe
a (a.u.)	10.263	10.692	10.300	10.684	10.711	10.222
a (Å)	5.431	5.658	5.451	5.654	5.668	5.409

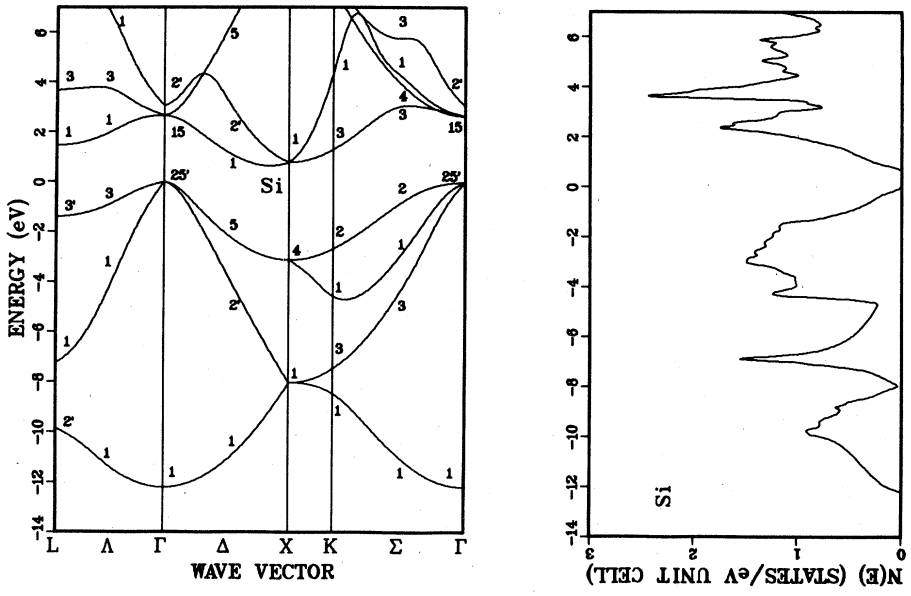

FIG. 1. Self-consistent energy bands and density of states for Si.

C. Comparison with other *ab initio* calculations

There is enormous literature on semiconductor band-structure calculations[1–25] of (with hindsight) varying quality. Some of the earliest successful calculations of Cohen and co-workers[1] and Herman and co-workers[5] were empirical in nature, fitting pseudopotential and OPW parameters to experimental optical and photoemission measurements. A number of other non-SC calculations[6–10] with various approximations to V_{xc} also exist. Several first-principles SC-OPW calculations[11–17] were performed for a number of semiconductors usually using a form of $V_{xc} = -3\alpha(3/\pi)^{1/3}\rho^{1/3}$, with $\alpha = \frac{2}{3}$, the Kohn-Sham value, or $\alpha = 1$, the Slater value. These SC-OPW calculations[11,17] were a *tour de force* in their time with the principal limitations being the difficulty of accurately including *d* electrons in the OPW method and, by today's standards, the crude approximation made for V_{xc}. Despite these

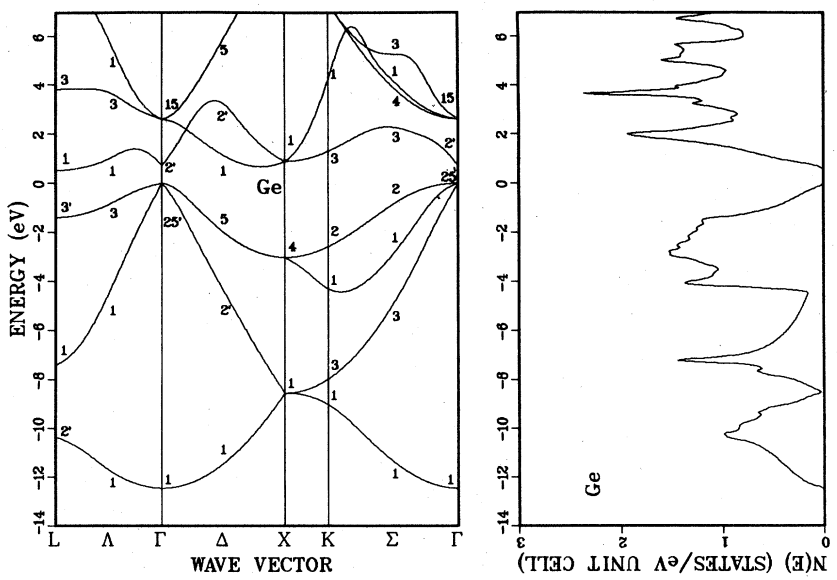

FIG. 2. Self-consistent energy bands and density of states for Ge.

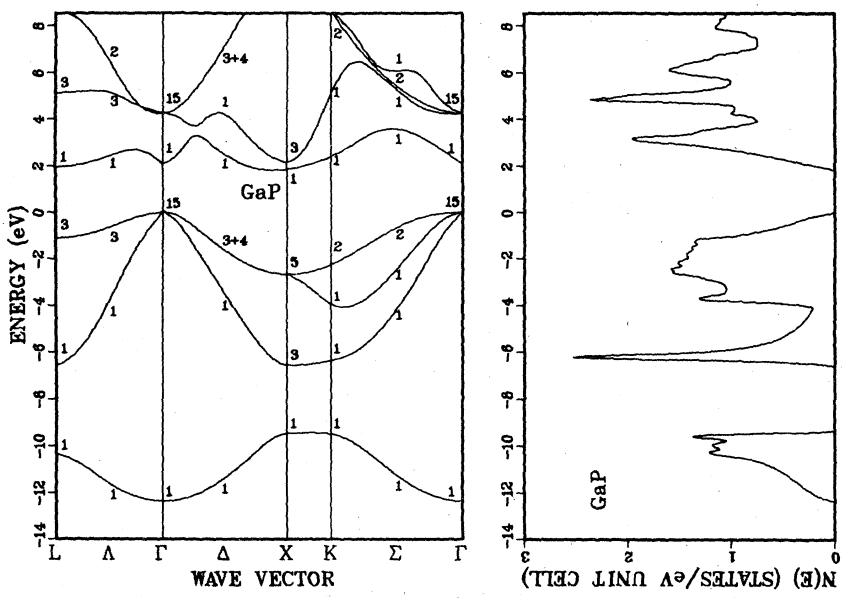

FIG. 3. Self-consistent energy bands and density of states for GaP.

limitations the discussions of relativistic effects,[11,17] particularly spin-orbit splitting by Wepfer *et al.*,[17] are a good source for ascertaining the quantitative relativistic corrections (up to several tenths of an electron volt) neglected in the present work.

More recently, a number of good quality SC calculations[22–24] have been performed with which we can compare. The difficulty in doing so in a meaningful way is due to various approximations often made to the crystal potential (e.g., spherical approximations), and also the different forms of V_{xc} used. Because of this we choose Si as an illustrative example, there being several SC calculations[12,23,24] with no shape approximation to the potential, and the V_{xc} are nearly the same as ours. We show the comparison in Table IV where we give our energy-band results for Si along with the LAPW results of Hamann[23] who used a V_{xc} very close to ours; the

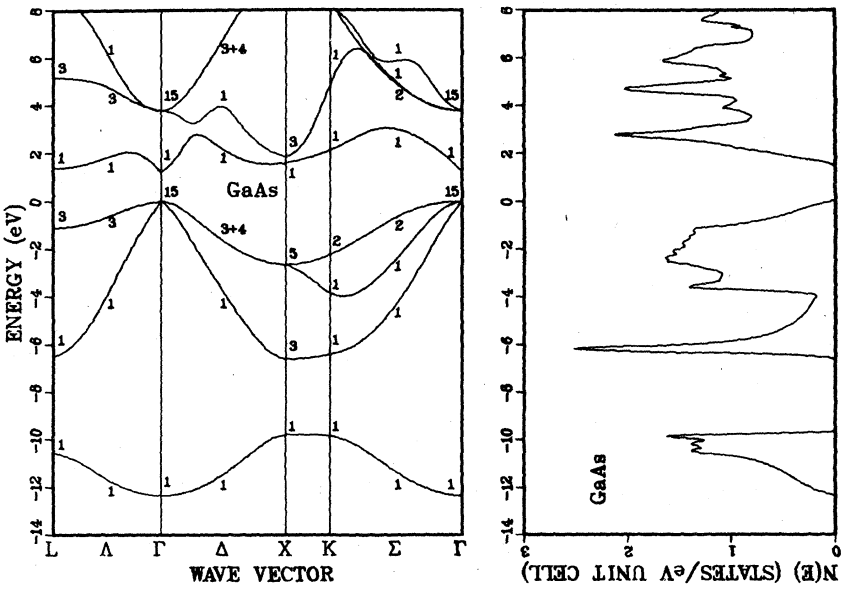

FIG. 4. Self-consistent energy bands and density of states for GaAs.

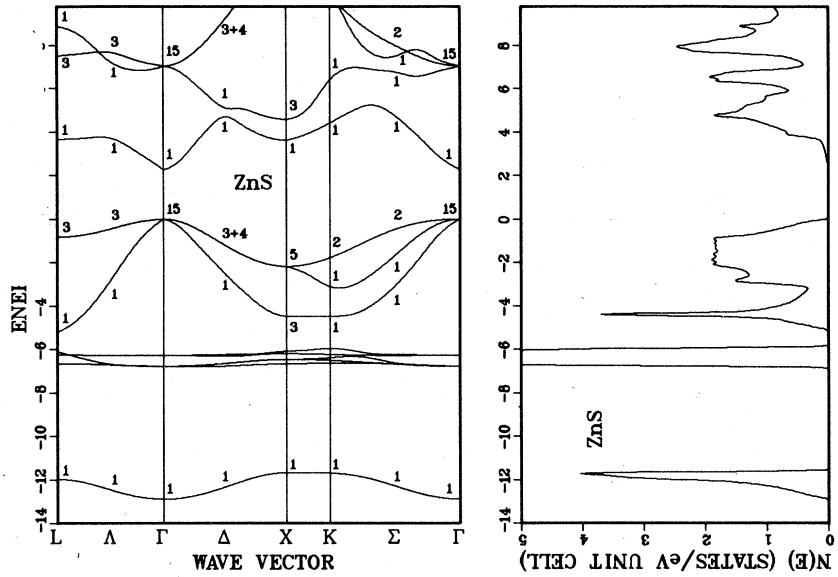

FIG. 5. Self-consistent energy bands and density of states for ZnS.

SC-pseudopotential results of Zunger and Cohen[24] who used the Hedin-Lundqvist LD form of V_{xc}, the SC-OPW results of Stukel and Euwema[12] for a V_{xc} of both $\alpha = 1$ and $\alpha = \frac{2}{3}$.

As can be seen from Table IV our results are in good agreement with the other SC calculations with the biggest disagreement being with the $\alpha = 1$ OPW results.[12] This is to be expected, as the latter is a large overestimate of the LD form of V_{xc} which (see Table IV) improves the calculated band gap, but pays the price of yielding somewhat inaccurate valence bands and presumably the charge density. The $\alpha = \frac{2}{3}$ OPW results[12] should be close to the LD forms of V_{xc}, and indeed these agree well with our results and those of Hamann[23] and of Zunger and Cohen.[24] We should emphasize an important conclusion of this comparison: All of the SC calculations using LD forms of V_{xc} underestimate the band gaps (as exemplified by X_1^c in Table IV) by $\sim 30\%$ or more. This underestimation of the band gaps is not an artifact of numerical band-structure approximations, but rather is a partial failure of the LD theory in describing excited states. Further discussions of the observed deviations from one-

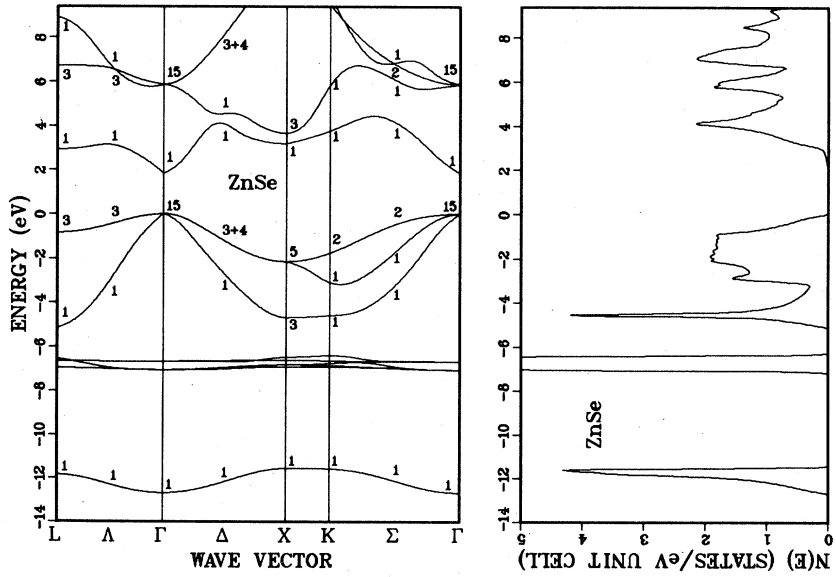

FIG. 6. Self-consistent energy bands and density of states for ZnSe.

TABLE II. Eigenvalues (eV) of lowest eight valence-conduction bands at Γ, X, and L. The top of the valence band is chosen as the zero of energy, and the Zn d bands have been excluded. Symbols in parentheses are symmetry labels. A more complete tabulation of eigenvalues on the 89-point mesh is given in Ref. 41.

$\Gamma(000)\frac{\pi}{a}$	$X(200)\frac{\pi}{a}$	$L(111)\frac{\pi}{a}$	$\Gamma(000)\frac{\pi}{a}$	$X(200)\frac{\pi}{a}$	$L(111)\frac{\pi}{a}$
	Si			Ge	
−12.20(1)	−8.03(1)	−9.86(2′)	−12.46(1)	−8.55(1)	−10.35(2′)
0.0(25′)	−3.11(4)	−7.25(1)	0.0(25′)	−3.03(4)	−7.39(1)
2.66(15)	0.79(1)	−1.40(3′)	0.72(2′)	0.88(1)	−1.40(3′)
3.05(2′)	10.11(3)	1.46(1)	2.61(15)	9.56(3)	0.52(1)
		3.66(3)			3.80(3)
		7.73(2′)			7.77(2′)
	GaP			GaAs	
−12.37(1)	−9.47(1)	−10.34(1)	−12.35(1)	−9.79(1)	−10.56(1)
0.0(15)	−6.58(3)	−6.57(1)	0.0(15)	−6.60(3)	−6.49(1)
2.05(1)	−2.68(5)	−1.11(3)	1.21(1)	−2.64(5)	−1.12(3)
4.26(15)	1.84(1)	1.95(1)	3.78(15)	1.61(1)	1.37(1)
	2.13(3)	5.10(3)		1.88(3)	5.15(3)
	10.83(5)	8.55(1)		10.26(5)	8.39(1)
	ZnS			ZnSe	
−12.89(1)	−11.67(1)	−11.97(1)	−12.67(1)	−11.55(1)	−11.83(1)
0.0(15)	−4.49(3)	−5.20(1)	0.0(15)	−4.69(3)	−5.15(1)
2.26(1)	−2.19(5)	−0.84(3)	1.83(1)	−2.16(5)	−0.85(3)
7.04(15)	3.61(1)	3.65(1)	5.86(15)	3.18(1)	2.91(1)
	4.58(3)	7.51(3)		3.64(3)	6.70(3)
	10.92(5)	8.87(1)		10.85(5)	8.91(1)

electron LD theory are given in Sec. IV and in paper II.

D. Relativistic effects

As mentioned previously our LCGO calculations are nonrelativistic, a good approximation since the maximum atomic number of the constituent elements in our study is 34 (for Se). However, relativistic corrections are not trivial so that we would like to point out several aspects of their effects. Two types of relativistic corrections occur: the scalar mass velocity and Darwin shifts, and shifts and splittings due to spin-orbit coupling. The former are discussed in some detail by Stukel *et al.*[11] and the latter by Wepfer *et al.*[17] in the context of the SC-OPW calculations referred to earlier. Another good discussion of the effects of relativistic corrections may be found in the work of Chelikowsky and Cohen[1] using empirical pseudopotentials.

Consider first the mass-velocity and Darwin corrections discussed by Stukel *et al.*[11] They find that the direct band gaps in ZnS and ZnSe are *decreased* by 0.3 and 0.6 eV, respectively, when these corrections are included. This occurs primarily because this gap is $\Gamma_{15}^{v}-\Gamma_{1}^{c}$, a transition between a p-like valence and an s-like conduction-band state, for which the scalar relativistic shifts should be different, with the s-like state being pulled down more than the p-like state. This should be a rather general result: Relativistic effects will tend to worsen the agreement between the theoretical and experimental band gaps.

Effects due to spin-orbit splitting are more complicated to discuss, but here we note that experimental values of Δ_0, the splitting of the $\Gamma_{25'}^{v}$, or Γ_{15}^{v}

TABLE III. Present theoretical and experimental direct (E_0) and indirect (E_g) for Si, Ge, and GaP band gaps in eV. Source of experimental results is Table 10-1 of Ref. 63.

	Theor.	Expt.
Si		
E_0 $(\Gamma^v_{25'} - \Gamma^c_{15})$	2.66	4.18
E_g $(\Gamma^v_{25'} - \Delta^c_1)$	0.65	1.13
Ge		
E_0 $(\Gamma^v_{25'} - \Gamma^c_{2'})$	0.72	0.89
E_g $(\Gamma^v_{25'} - L^c_1)$	0.52	0.76
GaP		
E_0 $(\Gamma^v_{15} - \Gamma^c_1)$	2.05	2.77
E_g $(\Gamma^v_{15} - \Delta^c_1)$	1.80	2.38
GaAs		
E_0 $(\Gamma^v_{15} - \Gamma^c_1)$	1.21	1.52
ZnS		
E_0 $(\Gamma^v_{15} - \Gamma^c_1)$	2.26	3.80
ZnSe		
E_0 $(\Gamma^v_{15} - \Gamma^c_1)$	1.83	2.82

states vary from ~ 0.04 eV for Si (Ref. 45) to ~ 0.45 eV for ZnSe.[46] These are nontrivial corrections which, however, likely have only a small effect on the calculated charge densities and photoemission spectra which we discuss in this paper.

IV. COMPARISON WITH PHOTOEMISSION MEASUREMENTS

One of the most widely used experimental probes of the semiconductor ground-state eigenvalues is photoelectron spectroscopy.[47] Within certain approximations, to be discussed, angle-integrated measurements of the energy distribution curves (EDC) can be compared with appropriately broadened densities of states, while angle-resolved photoelectron spectra (ARPES) give direct $E(\vec{k})$ results. EDC's obtained at x-ray[48–51] and ultraviolet[52–56] wavelengths (to be referred to as XPS and UPS, respectively), have been obtained for all of the semiconductors we have studied (only XPS for ZnS). Recently, accurate ARPES measurements have been reported for GaAs.[51,57,58]

In Fig. 7 we compare our theoretical $N(E)$ broadened with a Gaussian function of 0.7-eV full width at half maximum with the experimental[48–56] XPS and UPS EDC's. The broadening approximately accounts for the experimental resolution and electron lifetime effects. No matrix elements were included in the theoretical results so that the discrepancies in the absolute intensities were not meaningful. Although direct $E(\vec{k})$ information is not available from the EDC's, in the past the experimental data have been analyzed with the help of theoretical band-structure results (usually results of empirical pseudopotential calculations) to yield estimates of critical-point energies. In Tables V and VI we compare our critical-point energies with the so-determined experimental counterparts. Note that in Table VI we give the experimental and theoretical locations of the Ga and Zn $3d$ bands (not shown in Fig. 7) for comparison. Figure 8 shows our $E(\vec{k})$ curves along three symmetry lines along with the ARPES results for GaAs,[57,58] and Table VII compares the theoretical and experimental critical-point energies. We also include in Table VII the XPS-EDC values[50] for GaAs in order to indicate the differences that show up between these two measurements and their interpretations.

The agreement between our $E(\vec{k})$ results and the ARPES measurements for GaAs is quite good, with the largest deviations being the systematically higher (by $\sim 0.5-0.75$ eV) theoretical values of the low-lying narrow As s band. Although this discrepancy is not very large, it points up the nature of the corrections one must consider in comparing theoretical one-electron eigenvalues with photoemission measurements (see below). The overall qualitative agreement between our broadened $N(E)$ results and the XPS and UPS measurements is also very good. Here too, however, there are deviations which need to be explained. Experimentally, there is always some uncertainty with regard to determining the zero of energy (top of the valence band) which may explain the small uniform shifts of the experimental spectra with respect to our calculations [see, particularly, the ZnS results in Fig. 7(e)], but relative peak shifts need to be accounted for. These relative shifts are most apparent for the narrow lower valence bands (~ -12 eV) for the zinc-blende compounds, and particularly so for the Zn and Ga $3d$ levels. It appears that the largest theoretical-experimental

TABLE IV. Comparison of present LCGO eigenvalues (eV) with other *ab initio* self-consistent calculations for Si.

	Present work	LAPW[a]	OPW[b] $\alpha = 1$	OPW[b] $\alpha = \frac{2}{3}$	Pseudopotential[c]
Γ_1^v	−12.20	−12.02	−11.74	−12.04	−12.20
$\Gamma_{25'}^v$	0	0	0	0	0
Γ_{15}^c	2.66	2.49	2.79	2.33	2.48
$\Gamma_{2'}^c$	3.05	3.18	2.75	3.31	2.50
X_1^v	−8.03	−7.84	−7.75	−7.83	−8.02
X_4^v	−3.11	−2.82	−2.72	−3.00	−2.93
X_1^c	0.79	0.55	1.28	0.34	0.52
X_4^c	10.11	10.32	9.79	9.87	9.97
$L_{2'}^v$	−9.86	−9.64	−9.53	−9.63	−9.92
L_1^v	−7.25	−7.06	−6.75	−7.14	−7.21
$L_{3'}^v$	−1.40	−1.16	−1.18	−1.26	−1.26
L_1^c	1.46	1.40	1.60	1.39	1.39
L_3^c	3.66	3.37	3.83	3.12	3.12

[a]Reference 23.
[b]Reference 12.
[c]Reference 24.

disagreements occur for the relative separations of the higher extended valence bands and the lower lying more localized occupied states. The more these lower states are localized (narrower bands), the larger is the disagreement. The theoretical-experimental disagreements arise from the fact that the photoemission experiment is not a direct measure of a ground-state property. Rather, in photoemission one measures the total energy difference between an initial N-electron system and an $(N-1)$-electron system with an ejected electron. This total energy difference is usually approximated by the one-electron eigenvalue as we have done, but this is clearly an approximation which neglects relaxation effects around the hole and other many-body effects. For an isolated atom it is not difficult to calculate these total energy differences directly, but for a solid this type of calculation is not rigorously defined (see Ref. 59 for a detailed discussion of this point). Because of this we will here be content with a crude, but instructive discussion of these corrections.

In the case where an energy band is relatively unhybridized, one might expect that the corrections to the one-electron theory could be approximated by an atomic calculation. This is because in this case the band in question might be well approximated by its atomiclike character (s, p, d, etc.), whereby the corrections would correspond to a relatively uniform band shift. The relative corrections to the more localized bands such as the low-lying narrow s bands or the Zn $3d$ band versus the more extended upper valence p bands in the zinc-blende compounds can then be estimated by an atomic calculation. We have done this for GaAs using an atomic approximation for the As $4s$ and $4p$ states, calculating the total energy differences of the N and $N-1$ systems, comparing with the one-electron eigenvalues, and estimating the relative shifts between the s and p bands due to the many-body corrections.[60] We thus find a *relative* correction of ~ 0.8 eV lowering the $4s$ band into nearly perfect agreement (see Fig. 8) with the ARPES measurements. Similar estimates for the location of the Zn $3d$ band improves the theoretical-experimental agreement.[61] More rigorous ways of handling these kinds of corrections in a solid-state calculation are currently being studied by a number of groups. For the time being, the accurate calculation of excitation spectra in a one-electron, or a quasi-one-electron approach, is a questionable practice. As evidenced by the comparison with photoemission spectra here, and with optical spectra discussed fully in II, a number of theoretical improvements are needed.

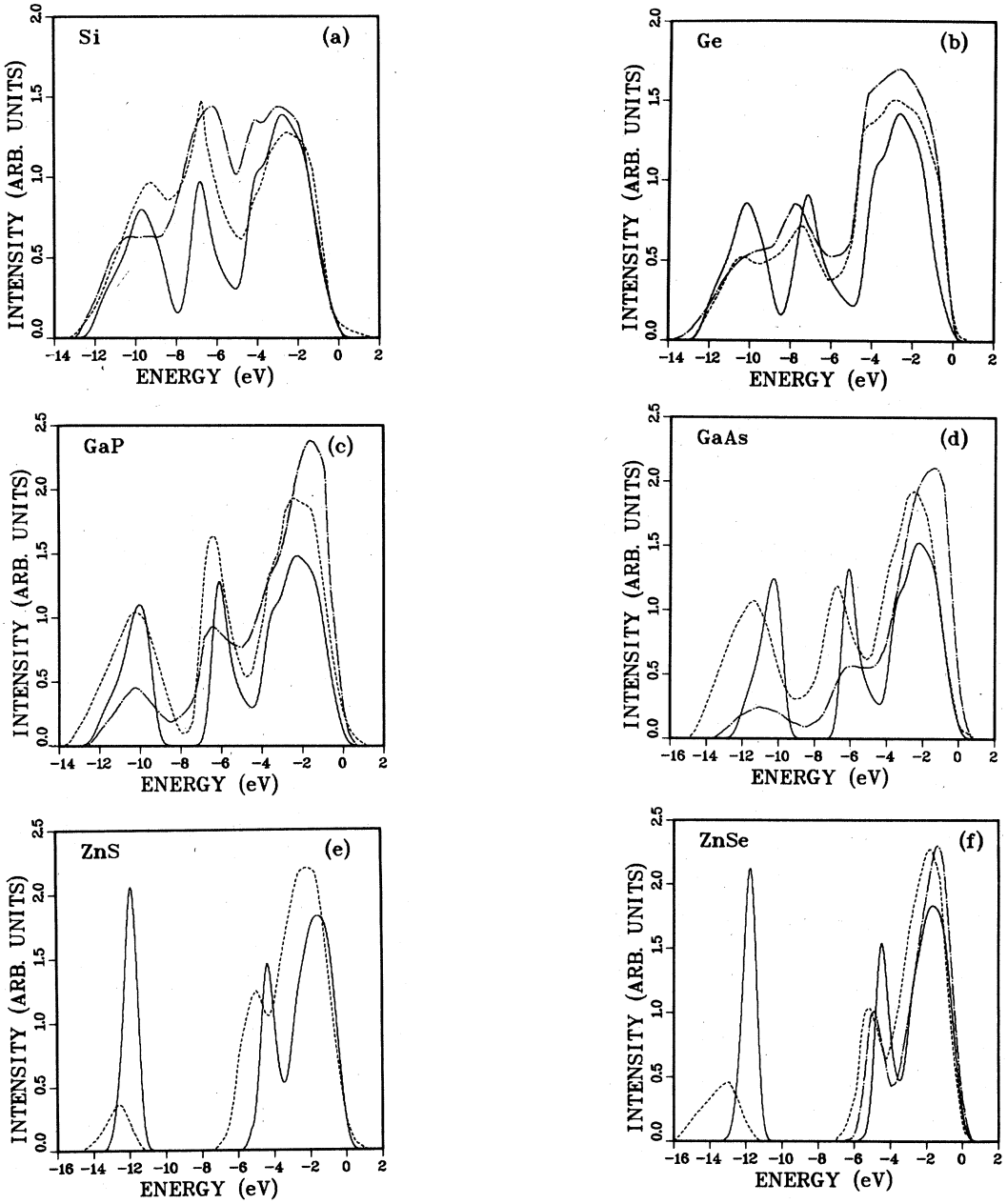

FIG. 7. Comparison of Gaussian broadened (FWHM = 0.7 eV) density of states (solid line) with experimental x-ray (dashed lines from Refs. 48—50) and ultraviolet (chain-dotted lines from Refs. 52—55) photoemission measurements: (a) Si, (b), Ge, (c) GaP, (d) GaAs, (e) ZnS, and (f) ZnSe.

V. EFFECTIVE MASSES

Effective masses of electrons and holes are important parameters in discussions of transport properties,[62,63] exciton effects, and electron-hole liquids in semiconductors,[64—67] to name a few. Values of effective masses can often be determined by, for instance, cyclotron resonances[68—71] or transport measurements.[62,72,73] In this section we present the results of our calculations of hole and electron effective masses at the valence-band maxima and the conduction-band minima of the six semiconductors that we have studied.

The effective masses are defined by

TABLE V. Comparison of the negative of the one-electron valence-band eigenvalues (eV) of Si and Ge, with the values inferred from angle-integrated photoemission measurements. In parentheses are the quoted experimental uncertainties where available.

	Si		Ge	
Feature	Theor.	Expt.	Theor.	Expt.
Γ_1^v	12.20	12.4(6)[b]	12.46	12.6(3)[a]
				13.0[c]
$L_{2'}^v$	9.86	9.2[c]	10.35	10.6(5)[a]
				10.3[c]
L_1^v	7.25	6.4(4)[b]	7.39	7.7(3)[a]
		6.6[c]		7.2[c]
$\Sigma_{1,\min}^v$	4.73	4.7(2)[b]	4.42	4.5(2)[a]
X_4^v	3.11	2.9[d]	3.03	3.2(2)[a]
L_3^v	1.40	1.2(2)[c]	1.40	1.4(3)[a]

[a]Reference 55.
[b]Reference 52.
[c]Reference 48.
[d]Reference 56.

TABLE VI. Comparison of the negative of the one-electron valence-band eigenvalues (eV) of GaP, GaAs, ZnS, and ZnSe, with the values inferred from angle-integrated photoemission measurements. In parentheses are the quoted experimental uncertainties where available. Theoretical values of the Zn $3d$ band energies are obtained from the maximum in the calculated density of states. The $3d$ bandwidths are 0.86 and 0.66 eV for ZnS and ZnSe, respectively.

	GaP		GaAs		ZnS		ZnSe	
Feature	Theor.	Expt.	Theor.	Expt.	Theor.	Expt.	Theor.	Expt.
Γ_1	12.37	13.2(4)[a]	12.35	13.8(4)[a]	12.89	13.5(4)[a]	12.67	15.2(6)[a]
		11.8(5)[b]		12.9(5)[b]				
L_1	10.34	10.6(3)[a]	10.56	12.0(5)[a]	11.97	12.4(3)[a]	11.83	13.1(3)[a]
X_1	9.47	9.6(3)[a]	9.79	10.7(3)[a]	11.67	12.0(3)[a]	11.55	12.5(4)[a]
		9.7(3)[b]		10.0(3)[b]				
L_1	6.57	6.9(2)[a]	6.49	7.1(2)[a]	5.20	5.5(2)[a]	5.15	5.6(3)[a]
X_3	6.58	6.9(3)[b]	6.60	6.9(2)[b]	4.49		4.69	5.3(3)[b]
W_1	6.35	6.5(2)[a]	6.40	6.6(1)[a]	4.42	4.9(2)[a]	4.54	5.2(2)[a]
$\Sigma_{1,\min}$	4.0	4.0(2)[a]	4.0	4.4(2)[a]	3.2	3.4(3)[a]	3.2	3.4(2)[a]
		4.1(3)[b]		4.1(2)[b]				3.4(3)[b]
W_2	3.61	3.6(2)[a]	3.52	4.0(2)[a]	2.76	3.0(2)[a]	2.80	2.6(2)[a]
X_5	2.68	2.7(2)[a]	2.64	2.5(3)[a]	2.19	2.5(3)[a]	2.16	2.1(3)[a]
L_3	1.11	1.2(3)[a]	1.12	1.4(3)[a]	0.84	1.4(4)[a]	0.85	1.3(3)[a]
		0.8(2)[b]		0.8(2)[b]				0.7(2)[b]
Ga(Zn)$3d$	15.6	18.55(10)[a]	15.8	18.82(15)[a]	6.4	9.03(15)[a]	6.7	9.20(15)[a]

[a]Reference 50.
[b]Reference 53.

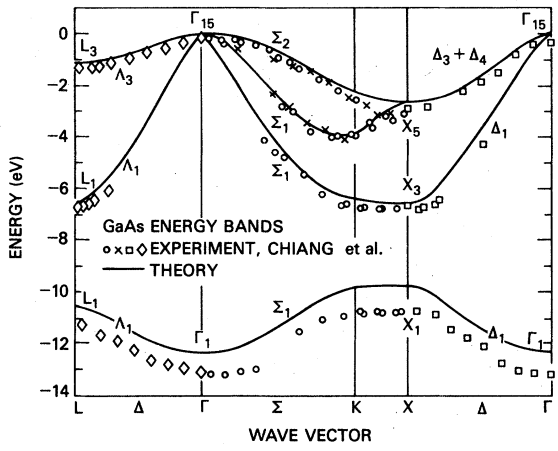

FIG. 8. Comparison of theoretical valence-band energies (solid lines) with experimental angle-resolved photoemission measurements of Ref. 58.

$$\frac{1}{m^*(\vec{k}_0)} = \left.\frac{\partial^2 E(\vec{k})}{\partial \vec{k}^2}\right|_{\vec{k}_0} \tag{6}$$

for a direction $\vec{k}$ about some point $\vec{k}_0$ in the Brillouin zone. The masses as defined in Eq. (6) can be determined using $\vec{k}\cdot\vec{p}$ perturbation theory,[63,71] but in our case it is particularly easy to evaluate the band energies at a sequence of points around $\vec{k}_0$ and evaluate m^* from Eq. (6) directly. This has been done for all of the $\vec{k}_0$'s in the following discussion. We now discuss the electron and hole masses separately.

A. Hole masses

The constant energy surfaces at the top of the valence band are warped cubes having highly direction-dependent effective masses.[62,63,71] Neglecting spin-orbit splitting as we have, the valence band-maxima at Γ are the triply degenerate $\Gamma_{25'}^v$ for Si and Ge, or Γ_{15}^v for the zinc-blende compounds. Two types of hole masses can be defined, heavy (h) and light (l) corresponding to the splitting of $\Gamma_{25'}^v$ (Γ_{15}^v) into a fairly flat doubly degenerate band (along Δ and Λ), and a more curved singly degenerate band, respectively. This can be seen clearly in Figs. 1—6. Since we have neglected spin-orbit coupling in our work we cannot say anything about the so-called split-off mass band resulting from the spin-orbit coupling. The calculated hole masses in the [100] and [111] directions are given in Table VIII, where we note the considerable anisotropy for the two directions. Average density of states hole masses can be defined by suitably averaging the direction-dependent masses over a number of angles. To do this we have followed the procedure of Lax and Mavroides[70,74] who make use of symmetry in defining the band energies close to Γ as

$$E(\vec{k}) = -k^2(A \pm B')\left[1 - \gamma\left[\frac{k_x^2k_y^2 + k_x^2k_z^2 + k_y^2k_z^2}{k^4} - \frac{1}{6}\right]\right] \tag{7}$$

and

$$m_{l,h}^* = \frac{1}{A \pm B'}\left(1 + 0.0333\gamma_{l,h} + 0.010\,57\gamma_{l,h}^2 - 0.000\,18\gamma_{l,h}^3 - 0.000\,03\gamma_{l,h}^4 + \cdots\right). \tag{8}$$

In Eqs. (7) and (8) the upper sign goes with the light mass and the lower sign goes with the heavy mass. As can be seen from Eqs. (7) and (8) the average light and heavy masses can be determined from the knowledge of $E(\vec{k})$ in two directions which we have chosen as the [100] and [111] directions. Table VIII lists the resulting average hole masses for all of the semiconductors along with the experimental results for Si (Ref. 75) and Ge,[76] and Lawaetz's[74] empirically determined values for the zinc-blende materials. Experimental results for the latter compounds are very sparse, and Lawaetz's values (his method gives very good agreement with experiment for the hole masses of Si and Ge) should be reasonably close to the true values. As can be seen from Table VIII, our theoretical average hole masses are systematically smaller than experiment or Lawaetz's values,[74] although the overall quantitative agreement is fairly good. Finally, we note that the experimental effective masses include effects due to the electron-phonon interaction (polarons) not accounted for in our bare band-structure masses. Theoretical estimates of these effects, which can change m^* by several percent, have recently been discussed by Beni and Rice,[77] and references therein.

B. Electron masses

The electron effective masses associated with the conduction bands are usually determined by cyclotron resonance or electroreflectance measurements, or from an analysis of transport data. For the semiconductors we have studied, there are two kinds of

TABLE VII. Valence-band critical-point energies, in eV, for GaAs.

	Theory[a]	ARPES[b]	XPS[c]
Γ_{15}^{v}	0	0	0
Γ_{1}^{v}	−12.35	−13.1	−13.8
L_{3}^{v}	−1.12	−1.30	−1.4
L_{1}^{v}	−6.49	−6.70	−7.1
L_{1}^{v}	−10.56	−11.24	−12.0
X_{5}^{v}	−2.64	−2.80	−2.5
X_{3}^{v}	−6.60	−6.70	−7.1
X_{1}^{v}	−9.79	−10.75	−10.7
$\Sigma_{1,\min}^{v}$	−4.0	−4.0	−4.4

[a]LCGO method, present work.
[b]Angle-resolved photoemission spectroscopy, Ref. 58.
[c]Angle-integrated x-ray photoemission spectroscopy, Ref. 50.

electron masses we discuss: one associated with the lowest conduction band at Γ, usually referred to as the cyclotron mass m_c^*, the second for the indirect-band-gap materials Si, Ge, and GaP, which are associated with the conduction-band minima along Δ for Si and GaP, and at L for Ge.

The cyclotron masses m_c^* we have determined are given in Table IX along with the values from the experiment where available.[78–81] As can be seen the agreeement between theory and experiment is generally good, with the largest discrepancies being for ZnS and ZnSe. We note that in the former case the experiment was done on a hexagonal phase of ZnS,[80] while for ZnSe the experimental error bar is $\pm$ 15%.[81]

For the indirect-gap materials we have found that the constant energy surfaces around the conduction-band minima are the well-known spheroidal surfaces for Si and Ge, and the same for GaP. In fact, we have found that the GaP surfaces have the same topology as Si, with six independent spheroids along the symmetry equivalent Δ axes. To our knowledge this is the first theoretical calculation to determine this structure for GaP, and the result has important consequences for interpreting experimental data and for theories such as electron-hole condensation. For Ge, there are four independent surfaces at L.

Two independent electron masses m_{eL}^* (L for longitudinal, parallel to the Γ-Δ-X axes for Si and GaP, and parallel to the Γ-L axis for Ge), and m_{eT}^* (T for transverse, perpendicular to the spheroidal axes) have been determined. Table IX lists our theoretical results along with the available experimental values.[82–84] The agreement is excellent, and we note our prediction of m_{eL}^* for GaP for which there are no direct measurements. The calculated total density of states mass for GaP $m_d^* = 6^{2/3}(m_{eL}^* m_{eT}^{*2})^{1/3} = 1.37$ agrees well with the value 1.21 ± 0.08 determined by Baranskii *et al.*[73]

TABLE VIII. Hole effective masses for carriers at the top (Γ) of the valence bands. Values quoted are in units of the free-electron mass. *lh* and *hh* stand for light and heavy holes, respectively. The first four columns give values of m^* for the $\vec{k}$-space directions indicated, while the theoretical and experimental values in columns five to eight are average values as discussed in the text.

	$m_{lh}^*[100]$	$m_{hh}^*[100]$	$m_{lh}^*[111]$	$m_{hh}^*[111]$	m_{lh}^* Theor.	m_{lh}^* Expt.	m_{hh}^* Theor.	m_{hh}^* Expt.
Si[a]	0.153	0.217	0.083	0.541	0.105	0.154	0.356	0.523
Ge[b]	0.037	0.199	0.031	0.512	0.033	0.042	0.332	0.347
GaP[c]	0.122	0.398	0.091	0.908	0.102	0.14	0.627	0.79
GaAs[c]	0.068	0.334	0.056	0.827	0.060	0.074	0.547	0.62
ZnS[c]	0.198	0.700	0.153	1.652	0.169	0.23	1.121	1.76
ZnSe[c]	0.139	0.546	0.110	1.243	0.121	0.149	0.859	1.44

[a]Experimental values from Ref. 75.
[b]Experimental values from Ref. 76.
[c]Experimental values are the semiempirical results of Lawaetz, Ref. 74.

TABLE IX. Electron (conduction-band) effective masses at Γ and along Δ, in units of the free-electron mass. m_c^* is the "cyclotron" mass at the lowest conduction-band Γ state. m_{eL} and m_{eT} are the longitudinal and transverse masses for Si, Ge, and GaP at the conduction-band minima (Δ,L,Δ, respectively). $\Delta_{\min}$ is the calculated fractional Γ-X distance of the location of the minimum for Si and GaP, and $\Delta E^{\min}$ is the calculated value of this minimum with respect to the X_1^c point.

	m_c^* Theor.	m_c^* Expt.	m_{eL}^* Theor.	m_{eL}^* Expt.	m_{eT}^* Theor.	m_{eT}^* Expt.	$\Delta_{\min}$	$\Delta E_{\min}$ (meV)
Si	0.158		0.915	0.916[e]	0.197	0.191[e]	0.846	138.2
Ge	0.037	0.038[a]	1.66	1.58[f]	0.088	0.082[f]		
GaP	0.127		1.25		0.24	0.25[g]	0.864	37.0
GaAs	0.070	0.066[b]						
ZnS	0.184	0.28[c]						
ZnSe	0.130	0.17[d]						

[a]Reference 78.
[b]Reference 79.
[c]Reference 80.
[d]Reference 81.
[e]Reference 82.
[f]Reference 83.
[g]Reference 84.

from an analysis of their experimental measurements on the temperature dependence of the carrier density in Te-doped GaP. There is also considerable interest in the values of $\Delta_{\min}$ and $\Delta E_{\min}$, the values of the location of the conduction-band minimum along the Δ direction, and the value of the energy of this minimum with respect to the X_1^c point, respectively. These values are also given in Table IX for Si and GaP.

IV. CHARGE DENSITIES AND FORM FACTORS

The valence electron charge densities for Si, Ge, GaP, GaAs, ZnS, and ZnSe are shown along the bond direction in Fig. 9 (solid lines) and as contour plots in the $(1\bar{1}0)$ plane in Fig. 10. They were calculated by summing $|\psi_n(\vec{k},\vec{r})|^2$ over all valence bands (index n) and sampling ten special $\vec{k}$ points[39] in the irreducible Brillouin zone. To be consistent with the results of the Ga compounds, the Zn 3d states, which lie more than 5 eV above the bottom of the valence bands with a dispersion of less than 1 eV, were not included. Note that the overall shapes of the charge-density contours for Si (Fig. 10) agree very well with previous theoretical studies[23,24] and with that constructed from the x-ray data.[85] The peak height of 21.3e/cell at the bond center is somewhat smaller than the experimentally derived value of 27.6, a result that was also found in earlier first-principles calculations[23,24] using the local-density approximation. Recently, Scheringer[86] has pointed out that Yang and Coppen's[85] value may be overestimated by as much as 3.6e/cell due to inaccuracies in the measured form factors[87] of four high momentum components. Note that our results for Si and Ge turn out to be extremely similar; their valence charge densities at the bond center are almost identical, although Si has a slightly more localized bond than Ge. Similar trends can be seen within the Ga and Zn compounds. Judging from the locations and heights of the bond charges (solid lines in Fig. 9), GaP and ZnS are more covalent and ionic than GaAs and ZnSe, respectively. As we move from the III-V to the more ionic II-VI compounds, the bond centers are shifted toward the anion sites, the maximum intensities increase, and the bonds become more localized.

Figure 11 displays our deformation densities (valence density minus a superposition of spherical, neutral, atom valence density used as starting values in our SC calculations) in the plane of the bond. Negative contours are dashed. It is interesting to note that the deformation charge bond densities for

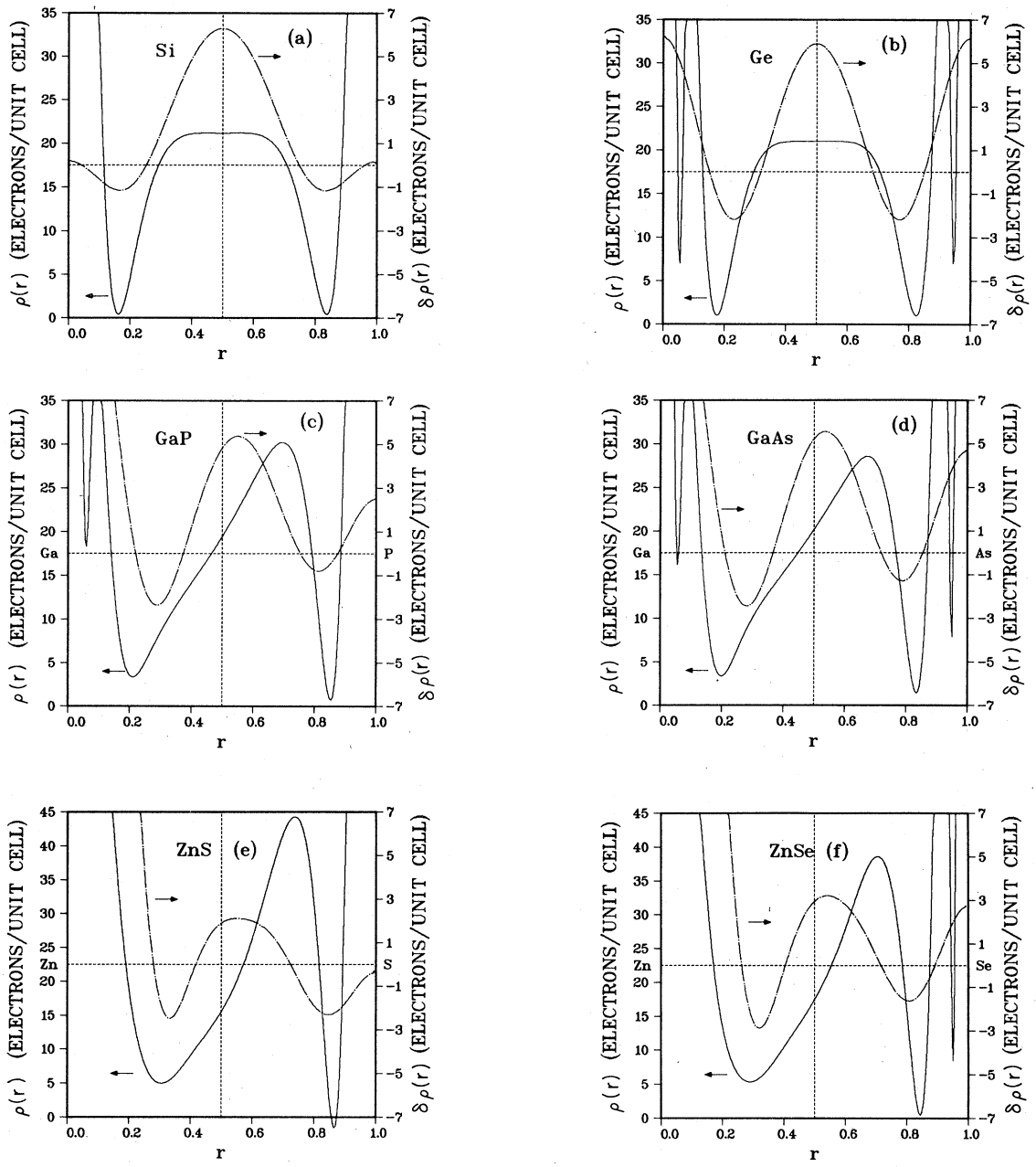

FIG. 9. Calculated valence $\rho(r)$ (solid lines) and $\delta\rho(r)$ (chain-dotted lines) along the [111] bonding direction: (a) Si, (b) Ge, (c) GaP, (d) GaAs, (e) ZnS, and (f) ZnSe. $\rho(r)$ is the self-consistent charge density, $\delta\rho(r)$ is the deformation density (self-consistent minus starting overlapping atomic charge densities), and r is the fraction of the nearest neighbor (bond) distance. The $3d$ bands of the zinc-blende compounds are not included.

Si and Ge are elongated perpendicular to the bond rather than along the bond direction as found in their valence densities (Fig. 10). The region of negative deformation charge is rather small indicating an overall increase of charge in this plane. Thus, a major effect of self-consistency is the buildup of charge along the bond as is to be expected in covalent semiconductors. For the zinc-blende materials, we note that the non-SC charge density derived from the potential of a superposition of overlapping, spherical, neutral, atomic charge densities already contains some degree of charge asymmetry in the bond.

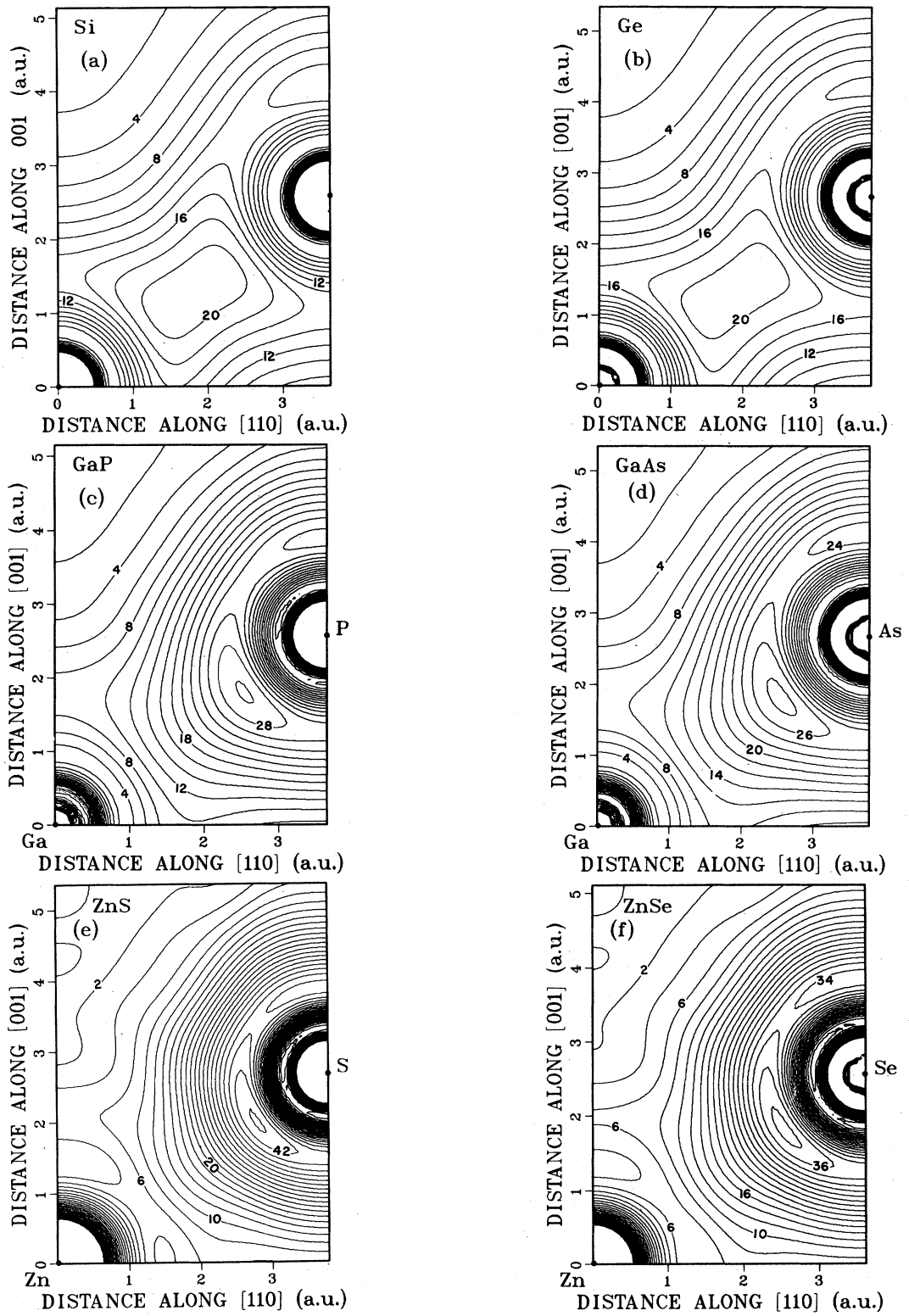

FIG. 10. Calculated self-consistent valence charge density in a portion of the $[1\bar{1}0]$ crystal plane for (a) Si, (b) Ge, (c) GaP, (d) GaAs, (e) ZnS, and (f) ZnSe. The contours are in units of electrons/unit cell, and the contour interval is two electrons/unit cell. The $3d$ bands of the zinc-blende compounds are not included.

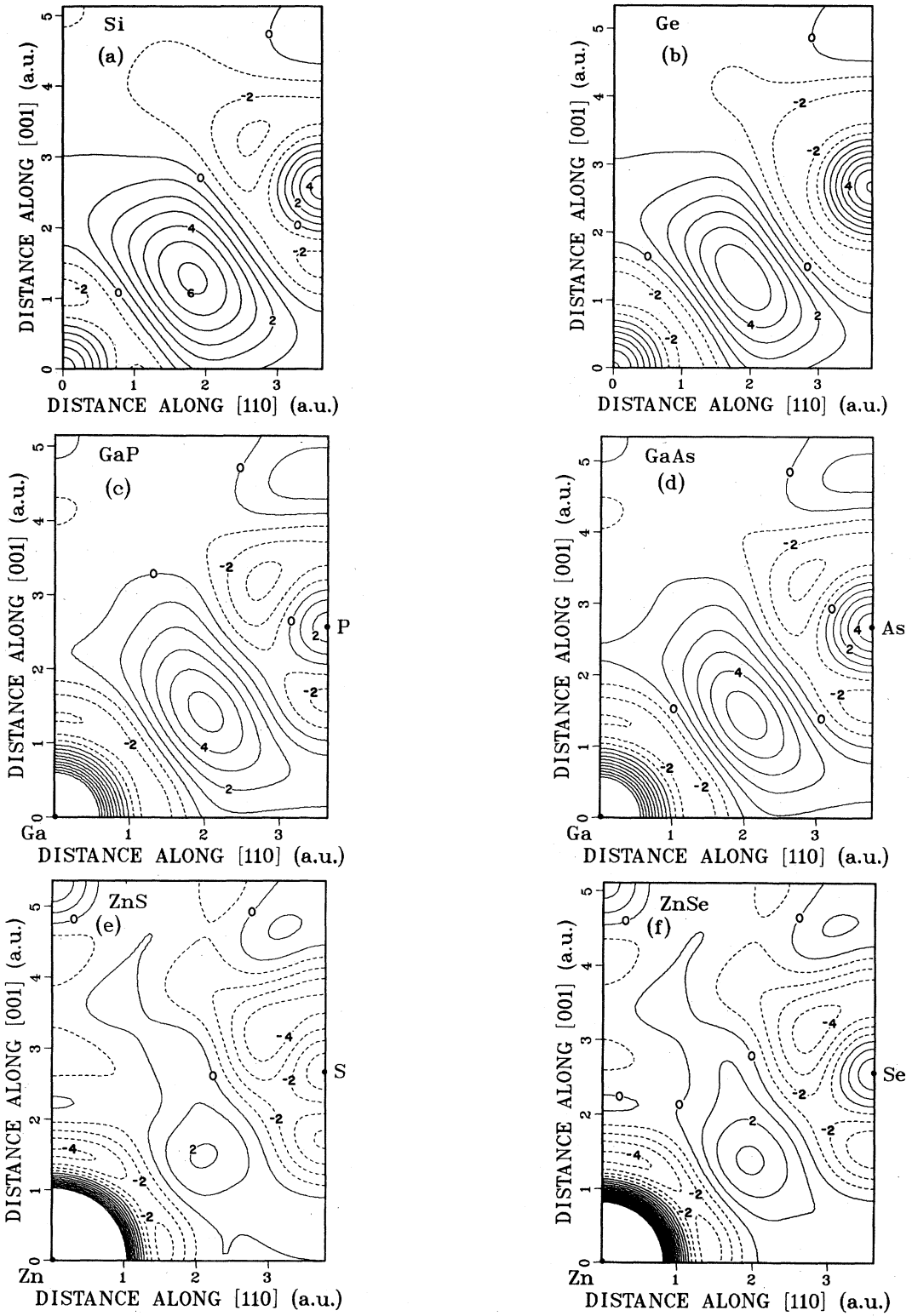

FIG. 11. Calculated deformation valence charge density (self-consistent minus starting overlapping atomic charge densities) in a portion of the $[1\bar{1}0]$ crystal plane for (a) Si, (b) Ge, (c) GaP, (d) GaAs, (e) ZnS, and (f) ZnSe. The contours are in units of electrons/unit cell, and the contour interval is one electron/unit cell. Negative contours are shown dashed. The *d* bands of the zinc-blende compounds are not included.

TABLE X. Comparison of experimental and theoretical form factors (in units of electrons/unit cell) for Si.

$\vec{K}(a/2\pi)$	Experiment[a]	Present	SC-OPW[b]	Pseudopotential[c]
[111]	15.19	15.11	15.12	15.13
[220]	17.30	17.26	17.28	17.14
[311]	11.35	11.37	11.33	11.02
[222]	0.38	0.25	0.34	0.38
[400]	14.89	14.92	14.88	14.70
[331]	10.25	10.17	10.20	9.94
[422]	13.42	13.37	13.36	13.30
[333]	9.09	9.07	9.02	8.92
[511]	9.11	9.08	9.08	8.98
[440]	12.08	12.04	12.04	12.00

[a]Reference 88 except for [222] which is from Roberto *et al.*, Ref. 89.
[b]Reference 87.
[c]Reference 24.

This explains why the corresponding deformation charge maps show more covalent character than ionicity when compared with their respective valence charge maps. Nevertheless, the bond center of the deformation charge density in Fig. 9 (broken lines) is shifted additionally towards the anion site in the zinc blendes studied.

A more direct comparison between theory and experiment can be made by examining the x-ray form factors. The choice of Gaussian orbitals as our basis functions enables us to evaluate the Fourier transforms analytically [Eq. (3)]. They are tabulated and compared with other theoretical estimates and available experimental data in Tables X–XIV for Si, Ge, GaP, GaAs, and ZnSe, respectively. All of the experimental results have been corrected for anomalous dispersion and to zero temperature. No experimental data are available for comparison for ZnS.

Si is the best studied material both theoretically and experimentally. Our results, which include the modification of the core wave functions in the crystal environment, are in excellent overall agreement with earlier SC-OPW calculation using a Kohn-Sham ex-

TABLE XI. X-ray form factors for Ge (in units of electron/unit cell).

$\vec{K}(a/2\pi)$	Experiment[a]	Present	SC-OPW[b]
[111]	39.42	38.83	38.95
[220]	47.44	47.23	47.26
[311]	31.37	31.29	31.21
[222]	0.26	0.22	0.48
[400]	40.50	40.56	40.54
[331]	27.72	27.39	27.53
[422]	36.10	35.91	36.00
[333]	24.50	24.35	24.34
[511]		24.35	24.38
[440]	32.34	32.23	32.32

[a]Reference 90.
[b]Reference 87.

TABLE XII. Absolute values of the x-ray structure factors for GaP (in units of electrons/unit cell).

$\vec{K}(a/2\pi)$	Experiment[a]	Present results
[111]	28.83	28.84
[200]	14.40	14.63
[220]	32.19	31.77
[311]	22.92	22.89
[222]	12.79	12.45
[400]	26.19	26.95
[331]	19.43	19.69
[420]	10.48	10.44
[422]	23.86	23.79
[333]	17.24	17.34
[511]	17.24	17.35
[440]	21.01	21.32

[a]Reference 91.

change potential.[87] The small differences compared with the first-principles pseudopotential results[24] may be due to the frozen atomic core approximation that they used and the procedure for core orthogonalization of the nodeless pseudowave functions. The agreement between our theoretical results and the experiment[88,89] is very satisfying. Generally, the theoretical-experimental differences

TABLE XIII. Absolute values of the x-ray structure factors for GaAs (in units of electrons/unit cell).

$\vec{K}(a/2\pi)$	Experiment[a]	Experiment[b]	Present results
[111]	39.44	39.06	38.85
[220]	47.18	46.66	47.18
[311]	31.37	31.04	31.25
[400]	40.84	40.40	40.44
[331]	27.75	27.45	27.32
[422]	36.22	35.84	35.80
[333]	24.37	24.10	24.30
[511]	24.54	24.27	24.30
[440]	32.38	32.04	32.15
[444]	26.94	26.66	26.77

[a,b]Reference 92. Two different anomalous dispersion corrections were used in reducing the experimental data. See Ref. 92 for details.

TABLE XIV. Absolute magnitude of the x-ray form factors for ZnSe (in units of electrons/unit cell).

$\vec{K}(a/2\pi)$	Experiment[a]	Present	SC-OPW[a]
[111]	39.64	38.99	39.06
[200]	3.72	2.99	2.79
[220]	47.45	47.16	47.37
[311]	32.28	31.23	31.38
[222]	2.91	2.55	2.38
[400]	40.58	40.27	40.63
[331]	27.39	27.23	27.59
[420]	3.02	2.82	2.77
[422]	35.14	35.63	36.11
[440]	32.19	32.06	32.55

[a]Reference 87.

are within the accuracy of the measurements. However, we feel that the disagreement for the (222) reflection is significant.

The (222) forbidden reflection has been the subject of intense investigation for many years.[89] Note that this term is a direct measure of the asymmetric charge distribution of the valence electrons around the atoms in the lattice. For example, an experimental value of 0.34 for $f(222)$ alone would contribute $2.7e$/cell to the charge density at the center of the Si—Si bond, while a superposition of overlapping spherical atomic Si charge densities would only yield $15.0e$/cell. Although our value $f(222) = 0.25$ is somewhat smaller than experiment and other theoretical estimates, our bond-charge maximum of $21.3e$/cell agrees very well with recent accurate LAPW calculations of Hamann ($22.2e$/cell) (Hamann's form factors are not given in Ref. 23). The first-principles pseudopotential method[24] yields a larger form factor (0.38) and also a larger bond maximum ($24.0e$/cell).

Table XI shows our results for Ge along with those from the earlier SC-OPW calculations[87] and experiments.[90] As for Si, the theoretical-experimental comparison is very gratifying except for the (222) forbidden reflection which once again shows the theory underestimating the experimental result.[90] We note that similar results were found in recent SC LCGO calculations for diamond,[32] where the theoretical value of $f(222)$ ($0.15e$/cell) was only half of the experimental measurement.

The calculated values of the absolute value of the

TABLE XV. Calculated real and imaginary parts of the Fourier coefficient of the charge densities (in units of electrons/unit cell) for the zinc blendes. The origin is at the cation, and the real part is followed by the imaginary part.

$\vec{K}(a/2\pi)$	GaAs		GaP		ZnS		ZnSe	
[111]	26.65	28.27	26.42	11.57	25.62	12.44	25.91	29.13
[200]	−1.48	0	14.63	0	13.06	0	−2.99	0
[220]	47.18	0	31.77	0	31.54	0	47.16	0
[311]	21.48	−22.70	21.12	−8.83	20.31	−8.86	20.76	−23.33
[222]	−1.20	0.19	12.45	0.19	11.21	0.10	−2.55	0.13
[400]	40.44	0	26.95	0	26.35	0	40.27	0
[331]	18.64	19.98	18.20	7.51	17.26	7.77	17.83	20.58
[420]	−1.39	0	10.44	0	9.23	0	−2.82	0
[422]	35.80	−0.02	23.79	−0.03	23.11	−0.04	35.63	−0.04
[333]	16.40	−17.93	15.92	−6.86	14.98	−7.16	15.57	−18.62
[511]	16.42	17.91	15.95	6.84	15.00	7.13	15.60	18.59
[440]	32.15	0	21.32	0	20.72	0	32.06	0

structure factors of GaP, GaAs, and ZnSe are shown in Tables XII–XIV along with the measured results[87,91,92] and, for ZnSe, the SC-OPW calculations.[87] Here, too, the theory and experiment compare favorably, although the agreement is not quite as good as for Si and Ge. Table XV lists our calculated values of the real and imaginary parts of the structure factors of all four zinc-blende com-

TABLE XVI. Directional anisotropy of charge and spin densities for transition metals by comparing the ratios of form factors for wave vectors of the same magnitude.

Element	Form factors	Wave vectors	Theor.	Expt.
Ni	Spin	$\frac{(3,3,3)}{(5,1,1)}$	2.179[a]	3.028[b]
Fe	Spin	$\frac{(3,3,0)}{(4,1,1)}$	2.351[c]	2.848[d]
Fe	Charge	$\frac{(3,3,0)}{(4,1,1)}$	1.0025[c]	1.010[e]
				1.011[f]
V	Charge	$\frac{(3,3,0)}{(4,1,1)}$	1.0039[g]	1.024[h]
				1.0085[i]

[a]Reference 29.
[b]Reference 93.
[c]Reference 30.
[d]Reference 94.
[e]Reference 95.
[f]Reference 96.
[g]Reference 31.
[h]Reference 97.
[i]Reference 98.

pounds. The origin is at a cation site, and the real part is followed by the imaginary part.

The discrepancies between our charge-density results and experiment (the theory gives a slightly too small bond charge and underestimation of the asphericity in the charge density) are probably related to the approximations inherent in local-density theory. Similar results have been found previously for the charge and spin densities in transition-metal systems (underestimation of asphericity) using various SC-LD approaches. In all *ab initio* calculations that we know of the asphericity, as mirrored in the form factors, is too small by 50% or more. To illustrate this point we show in Table XVI the theoretical ratios of form factors with the same magnitude of $\vec{K}$ for Ni,[29] Fe,[30] and V,[31] along with experimental results.[93–98] Additional experimental measurements for systems of varying degrees of covalency, ionicity, and metallicity would be useful for determining ways of improving the theory.

ACKNOWLEDGMENTS

We thank D. A. Papaconstantopoulos and W. E. Pickett for helpful discussions and comments on the manuscript, and Andrew Koppenhaver for technical assistance. This work was supported by the Office of Naval Research, Contact No. N00014-79-WR-90028.

[1]J. R. Chelikowsky and M. L. Cohen, Phys. Rev. B 14, 556 (1976). The empirical pseudopotential results here are widely used. References to earlier pseudopotential literature may be found in this paper.
[2]K. C. Pandey and J. C. Phillips, Phys. Rev. B 9, 1552 (1974).
[3]C. K. Kim and A. B. Kunz, Phys. Status Solidi 87, 765 (1978).
[4]M. Nishida, J. Chem. Phys. 69, 956 (1978).
[5]F. Herman, R. L. Kortum, C. D. Kuglin, J. P. Van Dyke, and S. Skillman, in *Methods in Computational Physics,* edited by B. Adler, S. Fernbach and M. Rotenberg (Academic, New York, 1968), Vol. 8.
[6]U. Rossler and M. Lietz, Phys. Status Solidi 17, 597 (1966).
[7]P. Eckelt, Phys. Status Solidi 23, 307 (1967); P. Eckelt, O. Madelung, and J. Treusch, Phys. Rev. Lett. 18, 656 (1967); P. Eckelt, Solid State Commun. 6, 489 (1968).
[8]O. Madelung and J. Treusch, in *Proceedings of the Ninth International Conference on the Physics of Semiconductors, Moscow, 1968,* edited by S. M. Ryvkin (Nauka, Leningrad, 1968), p. 38.
[9]R. C. Chaney, C. C. Lin, and E. E. Lafon, Phys. Rev. B 3, 459 (1971); S. Ciraci and I. P. Batra, *ibid.* 15, 4923 (1977).
[10]A. Seth and D. E. Ellis, J. Phys. C 10, 181 (1977).
[11]D. J. Stukel, R. N. Euwema, T. C. Collins, F. Herman, and R. L. Kortum, Phys. Rev. 179, 740 (1969).
[12]D. J. Stukel and R. N. Euwema, Phys. Rev. B 1, 1635 (1970).
[13]D. J. Stukel, R. N. Euwema, T. C. Collins, and V. H. Smith, Phys. Rev. B 1, 779 (1970).
[14]D. J. Stukel, Phys. Rev. B 3, 3347 (1971).
[15]T. C. Collins, D. J. Stukel, and R. N. Euwema, Phys. Rev. B 1, 724 (1970).
[16]D. J. Stukel, T. C. Collins, and R. N. Euwema, in *Electronic Density of States,* edited by L. H. Bennett, Special Publication 323 (Nat. Bur. Stand., Washington, D. C. 1971).
[17]G. G. Wepfer, T. C. Collins, and R. N. Euwema, Phys. Rev. B 4, 1296 (1971).
[18]J. Keller, J. Phys. C 4, L85 (1971).
[19]D. A. Papaconstantopoulos and B. M. Klein, Solid State Commun. 34, 511 (1980).
[20]B. Glotzel, B. Segall, and O. K. Andersen (unpublished).
[21]D. A. Papaconstantopoulos (unpublished).
[22]T. Jarlborg and A. J. Freeman, Phys. Lett. 74A, 349 (1979).
[23]D. R. Hamann, Phys. Rev. Lett. 42, 662 (1979).
[24]A. Zunger and M. L. Cohen, Phys. Rev. B 20, 4082 (1979).
[25]E. E. Lafon and C. C. Lin, Phys. Rev. 152, 579 (1966).
[26]R. C. Chaney, T. K. Tung, C. C. Lin, and E. Lafon, J. Chem. Phys. 52, 361 (1970).
[27]W. Y. Ching and J. Callaway, Phys. Rev. B 11, 1324 (1975); 9, 5115 (1974).
[28]S. P. Singhal and J. Callaway, Phys. Rev. B 16, 1744 (1977).
[29]C. S. Wang and J. Callaway, Phys. Rev. B 15, 298 (1977); J. Callaway and C. S. Wang, *ibid.* B 7, 1096 (1973).
[30]J. Callaway and C. S. Wang, Phys. Rev. B 16, 2095 (1977); R. A. Tawil and J. Callaway, *ibid.* B 7, 4242 (1973).
[31]D. G. Laurent, C. S. Wang, and J. Callaway, Phys. Rev. B 17, 455 (1978).
[32]R. Heaton and E. Lafon, Phys. Rev. B 17, 1958 (1978).
[33]C. S. Wang and J. Callaway, Comput. Phys. Commun. 14, 327 (1978).
[34]J. E. Simmons, C. C. Lin, D. F. Fouquet, E. E. Lafon, and R. C. Chaney, J. Phys. C 8, 1549 (1975).
[35]F. Herman and S. Skillman, *Atomic Structure Calculations* (Prentice-Hall, New York, 1963).
[36]R. N. Euwema, Phys. Rev. B 4, 4322 (1971).

[37]E. Wigner, Phys. Rev. 46, 1002 (1934).
[38]J. Callaway and J. L. Fry, in *Computational Methods in Band Theory,* edited by P. M. Marcus, J. F. Janak, and A. R. Williams (Plenum, New York, 1972), p. 512.
[39]D. J. Chadi and M. L. Cohen, Phys. Rev. B 8, 5747 (1973).
[40]O. Jepsen and O. K. Andersen, Solid State Commun. 9, 1763 (1971); G. Lehman and M. Taut, Phys. Status Solidi 54, 469 (1972).
[41]C. S. Wang and B. M. Klein, Naval Research Laboratory Memorandum Report No. 4482 (unpublished).
[42]D. E. Aspnes, C. G. Olson, and D. W. Lynch, Phys. Rev. Lett. 37, 766 (1976).
[43]D. E. Aspnes, Phys. Rev. B 14, 5331 (1976).
[44]D. S. Kyser and V. Rehn, Phys. Rev. Lett. 40, 1038 (1978).
[45]M. Cardona, K. L. Shaklee, and F. H. Pollak, Phys. Rev. 154, 697 (1967).
[46]J. L. Birman, H. Samelson, and A. Lempicki, G. T. & E. Res. Dev. J. 1, 2 (1961).
[47]*Photoemission in Solids I and II,* edited by M. Cardona and L. Ley (Springer, Berlin, 1978).
[48]L. Ley, S. Kowalczyk, R. Pollak, and D. A. Shirley, Phys. Rev. Lett 29, 1088 (1972).
[49]R. A. Pollak, L. Ley, S. Kowalczyk, D. A. Shirley, J. D. Joannopoulos, D. J. Chadi, and M. L. Cohen, Phys. Rev. Lett. 29, 1103 (1972).
[50]L. Ley, R. A. Pollak, F. R. McFeely, S. P. Kowalczyk, and D. A. Shirley, Phys. Rev. B 9, 600 (1974).
[51]K. A. Mills, D. Denley, P. Perfetti, and D. A. Shirley, Solid State Commun. 30, 743 (1979).
[52]W. D. Grobman and D. E. Eastman, Phys. Rev. Lett. 29, 1508 (1972).
[53]D. E. Eastman, W. D. Grobman, J. L. Freeouf, and M. Erbudak, Phys. Rev. B 9, 3473 (1974).
[54]W. D. Grobman and D. E. Eastman, Phys. Rev. Lett. 33, 1034 (1974).
[55]W. D. Grobman, D. E. Eastman, and J. L. Freeouf, Phys. Rev. B 12, 4405 (1975).
[56]W. E. Spicer and R. C. Eden, in *Proceedings of the Ninth International Conference of the Physics of Semiconductors, Moscow, 1968* (Nauka, Leningrad, 1968), Vol. 1, p. 61.
[57]T.-C Chiang, J. A. Knapp, D. E. Eastman, and M. Aono, Solid State Commun. 31, 917 (1979).
[58]T.-C Chiang, J. A. Knapp, M. Aono, and D. E. Eastman, Phys. Rev. B 21, 3513 (1980).
[59]J. P. Perdew and A. Zunger, Phys. Rev. B 23, 5048 (1981).
[60]The atomic calculations were done using the program of D. A. Liberman, D. T. Cromer, and J. T. Waber, Comput. Phys. Commun. 2, 107 (1971), with the Hedin-Lundqvist form of exchange correlation [L. Hedin and B. I. Lundqvist, J. Phys. C 4, 2064 (1971)]. The estimates given in the text should not be very dependent on the relativistic effects included in the program of Liberman *et al.*, nor on the slightly different form of exchange correlation from that in our other calculations (Ref. 37).
[61]F. J. Himpsel, D. E. Eastman, E. E. Koch, and A. R. Williams, Phys. Rev. B 22, 4604 (1980). This paper reports angle-resolved photoelectron spectroscopy experimental results and their interpretation of the energy bands of metallic Zn. Here, too, the LD theory does not give the correct location of the Zn 3*d* bands.
[62]C. Kittel, *Introduction of Solid State Physics,* 5th ed. (Wiley, New York, 1976).
[63]W. A. Harrison, *Electronic Structure and the Properties of Solids* (Freeman, San Francisco, 1980).
[64]T. M. Rice, Solid State Phys. 32, 1 (1978).
[65]J. C. Hensel, T. G. Phillips, and G. A. Thomas, Solid State Phys. 32, 88 (1978).
[66]G. Beni and T. M. Rice, Solid State Commun. 23, 871 (1977).
[67]G. Beni and T. M. Rice, Phys. Rev. B 2, 768 (1978).
[68]G. Dresselhaus, A. F. Kipp, and C. Kittel, Phys. Rev. 98, 368 (1955).
[69]J. M. Luttinger, Phys. Rev. 102, 1030 (1956).
[70]B. Lax and J. G. Mavroides, Phys. Rev. 100, 1650 (1955).
[71]C. Kittel, *Quantum Theory of Solids* (Wiley, New York, 1963).
[72]P. I. Baranskiĭ, A. E. Belyaev, and O. P. Gorodnichiĭ, Sov. Phys. Semicond, 10, 110 (1976).
[73]P. I. Baranskiĭ, O. P. Gorodnichiĭ, and A. U. Savchuk, Sov. Phys. Semicond. 10, 931 (1976).
[74]P. Lawaetz, Phys. Rev. B 4, 3460 (1971).
[75]J. C. Hensel and G. Feher, Phys. Rev. 129, 1041 (1963).
[76]J. C. Hensel and K. Suzuki, Phys. Rev. B 9, 4219 (1974).
[77]G. Beni and T. M. Rice, Phys. Rev. B 2, 840 (1977).
[78]R. L. Aggarwal, Phys. Rev. B 2, 446 (1970).
[79]R. Kaplan, M. A. Kinch, and W. C. Scott, Solid State Commun. 7, 883 (1969); G. E. Stillman, C. M. Wolf, and J. O. Dimmock, *ibid.* 7, 921 (1969).
[80]J. C. Miklosz and R. G. Wheeler, Phys. Rev. 153, 913 (1967).
[81]D. T. F. Marple, J. Appl. Phys. 35, 1879 (1964).
[82]J. C. Hensel, H. Hasegawa, and M. Wakayama, Phys. Rev. A 138, 225 (1965).
[83]B. W. Levinger and D. R. Frankl, J. Phys. Chem. Solids 20, 281 (1961).
[84]R. A. Stradling, Colloq. Int. C. N. R. S. 242, 317 (1975).
[85]Y. W. Yang and P. Coppens, Solid State Commun. 15, 1555 (1974).
[86]C. Scheringer, Acta Crystallogr. A36, 205 (1980).
[87]P. M. Raccah, R. N. Euwema, D. J. Stukel, and T. C. Collins, Phys. Rev. B 1, 756 (1970).
[88]P. J. E. Aldred and M. Hart, Proc. R. Soc. London Ser. A 332, 223 (1973).
[89]P. F. Price, E. N. Maslen, and S. L. Mair, Acta Crystallogr. A34, 183 (1978); J. B. Roberto, B. W. Batterman, and D. T. Keating, Phys. Rev. B 15, 2590

(1974); I. Fujimoto, *ibid.* 9, 591 (1974); B. Dawson and B. T. M. Willis, Proc. R. Soc. London Ser. A 298, 307 (1967).
[90]T. Matsushita and K. Kohra, Phys. Status Solidi 24, 531 (1974).
[91]R. Uno and J. Ishigaki, J. Appl. Crystallogr. 8, 578 (1975).
[92]T. Matsushita and J. Hayashi, Phys. Status Solidi A 41, 139 (1977).
[93]H. A. Mook, Phys. Rev. 148, 495 (1966).
[94]O. Terasaki, Y. Uchida, and D. Watanabe, J. Phys. Soc. Jpn. 39, 1277 (1975).
[95]M. Diana and G. Mazzone, Phys. Rev. B 9, 3898 (1974).
[96]J. J. DeMarco and R. J. Weiss, Phys. Lett. 18, 92 (1965).
[97]R. J. Weiss and J. J. DeMarco, Phys. Rev. 140, A1223 (1965).
[98]M. Diana and G. Mazzone, Philos. Mag. 32, 1227 (1975).